

Lawrence Berkeley National Laboratory

Recent Work

Title

THERMIONIC MISSION FROM PLANAR MONOCRYSTALLINE TUNGSTEN

Permalink

<https://escholarship.org/uc/item/0j097874>

Author

Schreiner, Sheldon Ira.

Publication Date

1966-06-01

UCRL-46699

University of California
Ernest O. Lawrence
Radiation Laboratory

THERMIONIC EMISSION
FROM PLANAR MONOCRYSTALLINE TUNGSTEN

TWO-WEEK LOAN COPY

*This is a Library Circulating Copy
which may be borrowed for two weeks.
For a personal retention copy, call
Tech. Info. Division, Ext. 5545*

Berkeley California

DISCLAIMER

This document was prepared as an account of work sponsored by the United States Government. While this document is believed to contain correct information, neither the United States Government nor any agency thereof, nor the Regents of the University of California, nor any of their employees, makes any warranty, express or implied, or assumes any legal responsibility for the accuracy, completeness, or usefulness of any information, apparatus, product, or process disclosed, or represents that its use would not infringe privately owned rights. Reference herein to any specific commercial product, process, or service by its trade name, trademark, manufacturer, or otherwise, does not necessarily constitute or imply its endorsement, recommendation, or favoring by the United States Government or any agency thereof, or the Regents of the University of California. The views and opinions of authors expressed herein do not necessarily state or reflect those of the United States Government or any agency thereof or the Regents of the University of California.

UCRL-16699

UNIVERSITY OF CALIFORNIA
Lawrence Radiation Laboratory
Berkeley, California

AEC Contract No. W-7405-eng-48

THERMIONIC EMISSION FROM PLANAR MONOCRYSTALLINE TUNGSTEN

Sheldon Ira Schreiner

(M. S. Thesis)

June 1966

THERMIONIC EMISSION FROM PLANAR MONOCRYSTALLINE
TUNGSTEN

Contents

Abstract

I. Introduction	1
II. Theory	3
III. Experimental Setup and Electrode Preparation	14
IV. Experimental Procedure and Circuitry	25
V. Presentation and Discussion of Results	28
VI. Conclusions	42
Acknowledgements	43
Appendices	
A. Nomenclature	44
B. Preparation of Single-Crystal Copper Collector and Guard Ring	45
C. THERM Code and Random Errors	47
References	49

THERMIONIC EMISSION FROM PLANAR MONOCRYSTALLINE TUNGSTEN

Sheldon Ira Schreiner

Inorganic Materials Research Division, of
Lawrence Radiation Laboratory,
University of California,
Berkeley, California

ABSTRACT

June 1, 1966

A thermionic diode and a vacuum system to test it were constructed to investigate the bare work function of (110) and (111) planar monocrystalline tungsten. The collector was (100) monocrystalline copper held at constant temperature. The work function for (110) tungsten was found to be 5.22 ± 0.01 V over the temperature range 2163 to 1697°K. For (111) tungsten the work function was found to be 4.74 ± 0.15 V over the range 2237 to 2013°K. At lower temperatures effects attributed to adsorption on the (111) surface were observed. The (100) copper work function was found to be 4.07 and 4.43 V for the two runs made but neither value is representative of a truly bare (clean) surface. The system pressure throughout the runs varied from 5×10^{-10} to 8×10^{-9} torr.

I. INTRODUCTION

Thermionic emission is the phenomenon associated with the imparting of sufficient thermal energy to some electrons in a metal cathode to enable them to overcome retarding forces at the surface of the metal and thus be emitted. A thermionic emission diode is formed by collecting the electrons on an anode.

The thermionic parameter of importance is the bare work function. It is the energy difference an electron experiences in going from the Fermi level in a metal to a position at rest in field free space. It is important to realize that the work function is dependent upon the surface properties as well as the interior properties of the lattice.

I investigated the bare work function of (110) and (111) single-crystal tungsten emitting surfaces, using a temperature-controlled (100) single-crystal copper collector. A lot of work has been done on single crystal wire and hemispherical crystals¹⁻⁷ but very little has been done on planar crystals.^{8,9} My experiments were motivated, in part, by uncertainties arising from the work of Koenig¹⁰ on single-crystal tungsten emitters with a polycrystal copper collector. Aside from determining the respective single-crystal bare work functions of tungsten and copper, I hoped that these experiments will better explain thermionic emission observed when the collector is maintained at a constant temperature. This should allow us to decide what effects are due to a change in emitter work function with temperature.

The theory needed to analyze these experiments is presented in Chapter II. Chapter III describes the experimental setup and the electrode preparation. Chapter IV describes the experimental procedure and

the circuitry employed. The results are presented and discussed in Chapter V and the conclusions given in Chapter VI. The appendices contain a list of symbols and their definitions, a more complete discussion of the collector preparation, and a discussion of the THERM code used in all data reduction.

II. THEORY

The three regions of interest in a thermionic diode are: the emitting cathode, the interelectrode gap, and the collecting anode. Let us restrict our attention to them and closely examine the physics of thermionic emission diodes. We will then be in a position to see how a proper analysis of the experimental data will yield the desired parameters of interest.

The process of thermionic emission from metals involves the relative positions of three electronic energy levels, namely, according to the Sommerfeld model, the bottom of the conduction band, the Fermi level, and free space. The bottom of the conduction band, E_c , is defined as the lowest energy that a free electron can have in the metal. If we choose this energy level as our reference, $E_c = 0$, then the energy level of an electron at rest in the field free space is W , where W is the height of the potential barrier at the surface of the metal. The Fermi level of the metal, F , is defined as the energy state, relative to the bottom of the conduction band, having a 50% probability of occupancy. The work function, ϕ , associated with a metal and its interface with free space is defined as the change in energy that an electron experiences in going from the Fermi level in the metal to a position at rest in field free space, an infinite distance from the surface, that is

$$e\phi = W - F, \quad (1)$$

where e is the charge on the electron and 10^{-7} meters constitutes an infinite distance. Because this distance is so small, the surface of the metal is often characterized by a step change in a potential energy, or motive, diagram as shown in Fig. 1. ¹¹

For crystalline solids, W and F are functions of the crystallographic orientation, so in order to define the work function, one must specify the crystallographic orientation of the surface through which the electron passes. In addition, the work function is influenced strongly by the presence of adsorbed layers of foreign matter on the surface, so the extent of surface contamination must be described also.

An electron travelling from the emitter to the collector encounters a field due to all of the electrons in the space between the electrodes and the potential difference between the electrodes. If the electron density in this space is high enough, the current that reaches the collector will be determined by these charges rather than by the work function and temperature of the emitter. The current is then said to be limited by space charge. There are three ways to eliminate space charge: decrease the gap size, apply an accelerating potential across the gap, or reduce the currents to very small amounts.

When the current is limited by space charge, the charges in the space increase the height of the potential barrier surrounding the emitter which the electrons must cross in travelling to the collector. The smaller the gap between the electrodes, the smaller the distance the space charge has to build up in and thus the smaller the effect on saturated emission. If an accelerating potential of sufficient strength is applied to the collector, the current is no longer limited by the charges in the space but is determined by the work function and temperature of the emitter. The current is then said to be saturated or emission limited. If the accelerating potential is not strong enough, then we do not get saturated emission and we cannot make any statements about the emitter parameters. In practice, however, it is possible to extrapolate

the data to give the saturated emission situation. The smaller the effect of space charge, the more reliable the extrapolation.

When assimilated by the collector, the electrons give up a binding energy $e\phi_c$ in the metal (where ϕ_c is the work function of the collector metal) and a voltage V when they pass through an external load.

Fundamental to the understanding of vacuum diode performance is the concept of the motive diagram put forward by Langmuir (see Fig. 1). The changes in potential energy of the electron depend on all the forces acting upon it. The motive diagram shows graphically the potential energy of an electron as it goes from the interior of the emitter, through the interelectrode gap, to the interior of the collector.¹² Figure 1a corresponds to the retarded region where those emitted electrons with energy less than V_a do not reach the collector. In Fig. 1b the electrons have just enough energy for all of them to get to the collector, producing a saturated current. Superimposed on the diagram is the retarded potential distribution (δ) the electron would have to overcome in the presence of space charge. And, in Fig. 1c we have superimposed the accelerating potential, V_a , measured with respect to the grounded emitter onto Fig. 1b to increase the electron collection by the anode and overcome space-charge effects.

In Fig. 1, δ - Space charge barrier

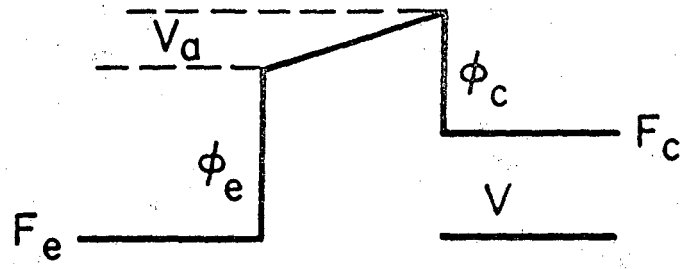
ϕ_e, ϕ_c - Emitter and collector work function

V_0 - Contact potential voltage = $\phi_c - \phi_e$

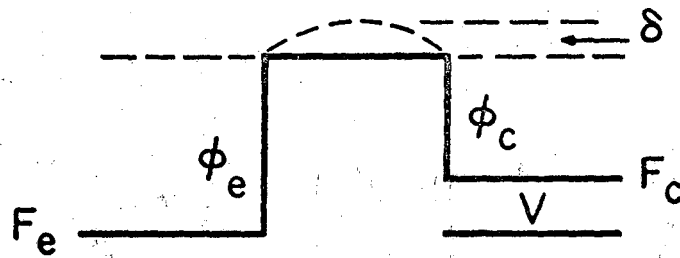
V - External voltage measured between electrodes

V_a - Interelectrode voltage

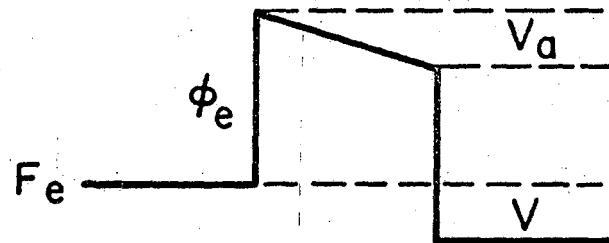
F_e, F_c - Emitter and collector Fermi level



(a)



(b)



(c)

MUB-10639

Fig. 1. Motive diagram. (a) Retarded region, $V_a = V + V_0$; (b) critical point, $V = -V_0$; (c) saturated region, $V_a = V - V_0$.

We are now in a position to give a quantitative analysis of thermionic emission and to show how the various constants of interest are determined experimentally. First a plot is prepared in the manner shown in Fig. 2 to record the logarithm of the current density, J , as a function of the applied voltage, V , for different values of the emitter temperature, T_e . Over many orders of magnitude of current density, this logarithm will be a linear function of the applied voltage; this is the "retarded region". At a critical value of the applied voltage, V_0 , this linear plot joins tangentially to a curve characteristic of the "saturated current region". In Fig. 2 we see how the current and voltage behave experimentally to correspond with the physics in Fig. 1.

From the slope of the line in the retarded region the true electron temperature of the emitter is determined. This is true only in the absence of space charge and if both electrodes have uniform work functions. The equation for this line is

$$J = J_0 \exp(eV/kT), \quad (2)$$

where

J = current density

J_0 = saturated emission current density corresponding to
 $\phi_e = \phi_c$

V = measured voltage

k = Boltzmann constant

T = absolute temperature of electrons

Any two points on the line will enable us to determine the electron temperature. Theoretically the electron temperature and the emitter temperature should be equal, but in practice the electron temperature is greater. This difference can be explained by Fig. 2. Any departure

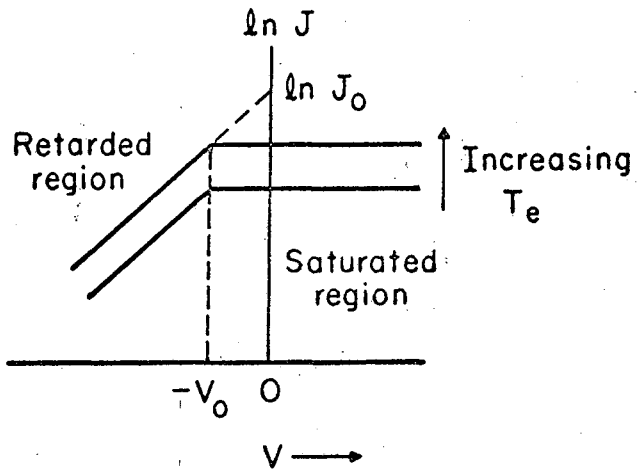


Fig. 2

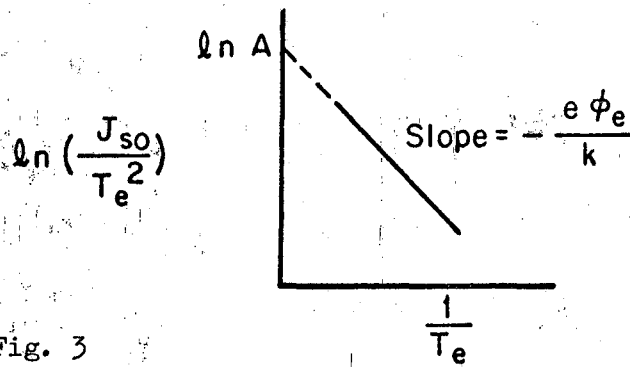


Fig. 3

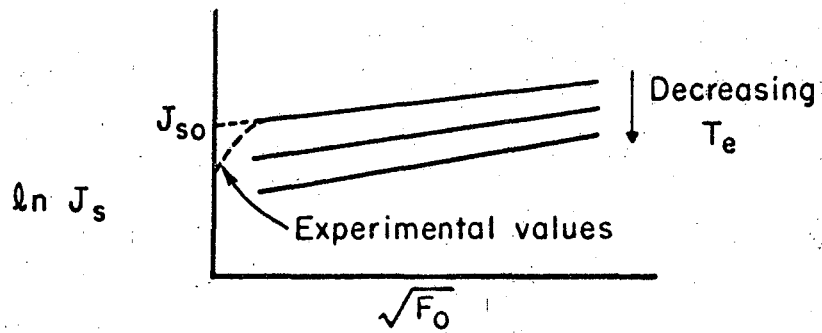


Fig. 4

MUB-10640

- Fig. 2. Current-voltage characteristics.
- Fig. 3. Richardson plot.
- Fig. 4. Schottky plot.

from ideal emission will result in a rounding of the curve at V_0 . This will produce a more shallow slope of the line in the retarded region and thus give rise to a greater electron temperature. This is exactly what occurs in the presence of space charge. As mentioned earlier, it is possible to extrapolate the two lines to their point of intersection, if the curve is rounded, and thus calculate a theoretical V_0 .

The above conclusion about the physical significance of T requires one basic assumption -- constant collector work function. The work function can change from temperature variations of the collector or from collector surface heterogeneity.¹³⁻¹⁵ In our experiment the collector was cooled in order to maintain it at a constant temperature.

We have shown that the bare work function -- i.e., emission from clean surfaces -- is quite different for different faces of a metal crystal.^{8,16} Yet, in the foregoing discussion we have tacitly assumed that the emitting surface has a uniform work function, implying that only a single crystal face is exposed on the electrode surface. In a metallic crystal, the center of gravity of the electron cloud in each cell coincides with the atomic nucleus, and therefore the dipole moment of these cells is equal to zero. For cells at the surface of the metal, the situation is different. Here, the electron cloud is not symmetric with respect to the atomic nucleus; it extends towards the exterior by a distance about equal to the difference in the atomic radii in a gas-like state and in the crystal lattice. Therefore, each cell of the crystal has a dipole moment and all the surface cells form a double electric layer. The moment of a single cell depends on the structure of the boundary surface of the given crystal, and hence the moments of the double layers on the different faces of a single crystal are not identical.

This accounts for the nonuniformity of the work function of a polycrystalline surface. Therefore, to ensure a uniform collector work function, a single crystal of copper with a (100) orientation was used for the collecting electrode.

The critical condition at the knee of the curve corresponds to the situation in Fig. 1b, which gives us the relation

$$V_o = \phi_c - \phi_e \quad (3)$$

This value of the voltage is known as the contact potential. Knowing V_o and one of the work functions, we can directly calculate the other.

The expression that relates the saturated emission current drawn from an emitting surface with the work function and temperature is the Richardson-Dushman equation¹⁴

$$J_{so} = A(1-\bar{r}) T_e^2 \exp(-e\phi_e/kT_e), \quad (4)$$

where J_{so} = saturated current density (amperes/cm²) at zero applied field

\bar{r} = the average reflection coefficient for electrons at the emitter surface

A = Richardson constant = $\frac{4\pi emk^2}{h^3} = 120 \text{ amperes/cm}^2 \text{-}^\circ\text{K}$,
theoretically,

m = mass of electron

h = Planck constant

T_e = temperature of emitter ($^\circ\text{K}$)

ϕ_e = work function of emitter (Volt).

The average reflection coefficient has been shown to be negligibly small and is taken as zero.¹⁵ If we plot $\ln(J_{so}/T_e^2)$ as a function of $1/T_e$, we get the Richardson plot

$$\ln(J_{so}/T_e^2) = \ln(A) - e\phi_e/kT_e \quad (5)$$

The slope of this line is $-e\phi_e/k$ and the intercept with the ordinate axis is $\ln(A)$, as shown in Fig. 3.

The Richardson-Dushman equation was derived on the basis of a zero applied field, a condition not experimentally satisfied. Also, we cannot tell if the A we get from a Richardson plot is temperature dependent or not. A further discussion on evaluating A is given below.

Experimentally and theoretically it is found that the emission current increases with increasing field strength at the emitter. This effect, known as the Schottky effect, indicates that the work function of the cathode depends upon the surface field strength. This is caused by the electron in front of the surface being acted upon by its own electrical image in the metal.¹⁷

It can be shown that the current in the presence of a small field, F_o , is given by¹⁷

$$J_s = J_{so} \exp\left(\frac{e}{2} \sqrt{\frac{eF_o}{\pi\epsilon_o}} \frac{1}{kT}\right), \quad (6)$$

where F_o is the field and J_s is the emission current density for nonzero field strength. Hence, plotting $\ln J_s$ versus $\sqrt{F_o}$ should give us a straight line whose intercept at $F_o = 0$ is J_{so} . This plot is known as a Schottky plot as shown in Fig. 4. The Schottky effect is observed most clearly at relatively low temperatures because of the $1/T$ dependence of the exponent. The experimental points fall off at low fields due to space charge and field inhomogeneities.

Therefore, in order to properly analyze our data to get ϕ , we should first make a number of Schottky plots for different temperatures, determine J_{so} for each plot by extrapolating to zero field, and then plot $\ln(J_{so}/T_e^2)$ versus $1/T_e$. The value of A and ϕ_e we get out of this plot we will call

A_R and ϕ_R .

However, we still have to take account of temperature dependence on A_R and ϕ_R . This is accomplished by making a Shelton plot,¹⁸ it is essentially a Richardson plot of $\ln(J/T_e^2)$ versus $1/T_e$ for the collector work function, ϕ_c , made by plotting the data from the current-voltage characteristics of Fig. 2 in the retarded region for a constant applied voltage, i.e., a constant retarded potential barrier. Therefore, if the collector work function is maintained at a constant temperature, a straight line will result where the intercept gives the true value of A denoted by A^* . Note, though, that this is true only when the Boltzmann temperature calculated from the slope of the retarded region equals the temperature of the emitter, determined by the pyrometer.

Finally, we can now take A^* from the Shelton plot, and J_{so} from the Schottky plot, and recalculate ϕ_e from the Richardson equation. What we now get is the "true work function" for the emitter. By this is meant the work function that corresponds with our definition in Eq. (1). If it agrees with ϕ_R then we know ϕ_R is temperature independent; if it differs then we know ϕ_R is temperature dependent and we can calculate this dependence to first order by assuming the first two terms in a Taylor series expansion.

Experimentally, it is known that the dependence of the work function upon temperature is very small. This allows us to express it in the simplest way, assuming a linear dependence of the form

$$\phi_e = \phi_{e0} + \alpha(T_e - T_0), \quad (9)$$

where

ϕ_e = the temperature-dependent emitter work function

ϕ_{e0} = the emitter work function at the temperature of reference T_0

$\alpha = d\phi_e/dT_e$ is the temperature dependence of ϕ_e
 T_e = the emitter temperature.

Putting Eq. (9) into Richardson's equation we can write

$$J_{so} = A_R \exp(-e\phi_{e0}/kT), \quad (10)$$

where $A_R = A^* \exp(-e\alpha/k)$, A^* is known from the Shelton plot, and we have taken $T_0 = 0^\circ\text{K}$. Thus we see that from the initial Richardson equation we could not determine the true Richardson constant and emitter work function because of possible temperature dependence. The ϕ_R we calculated was really ϕ_{e0} .

Since experimenters are having trouble getting the Richardson A, a convention has been taking hold of putting A equal to 120 amperes/cm²-°K² into the Richardson equation and calculating a work function at each temperature. This work function is then called the "effective work function," ϕ_{eff} .

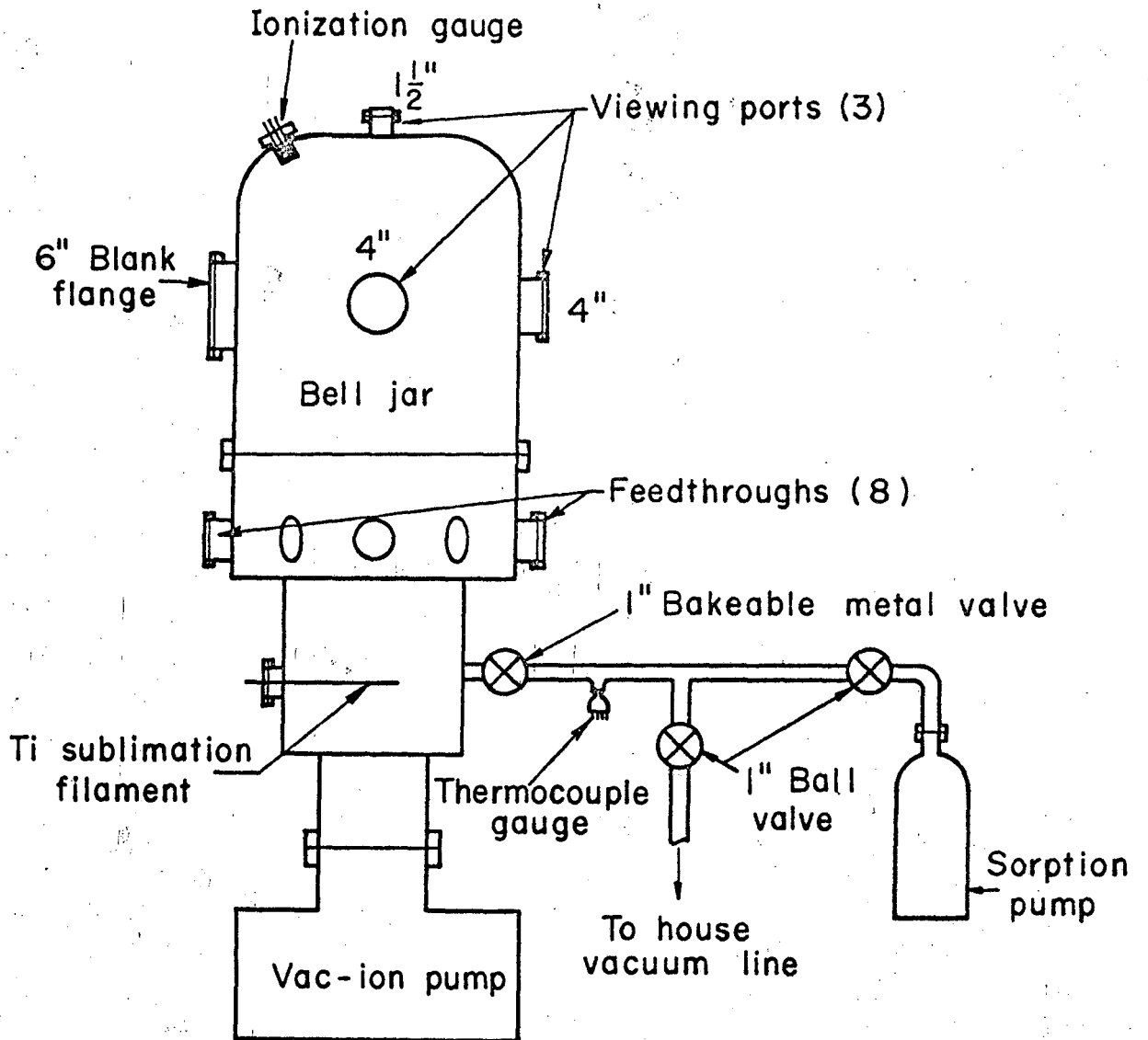
In summary, then, we (a) draw the current-voltage characteristics in order to get the true electron temperature and the contact potential, (b) draw a Schottky plot to get the saturated current density at zero applied field, (c) draw a Shelton plot to get the true value of the Richardson constant and the collector work function, (d) using the Richardson constant from the Shelton plot and the saturated current density from the Schottky plot we can then get the true emitter work function from the Richardson equation and finally (e) assuming a linear temperature dependence for the emitter work function we can calculate its temperature dependence to first order.

III. EXPERIMENTAL SETUP AND ELECTRODE PREPARATION

We built a vacuum system in which to conduct the experiments. It is mounted on a movable instrumentation stand. The diode, resting on a stainless steel support stand inside the bell jar, is positioned so that the gap between the electrodes can be viewed from two ports positioned 90° apart.

The vacuum system pictured in Figs. 5 and 6 is made of 3/16-inch-thick stainless steel. The bell jar is 12 inches in diameter and 15 inches high. Below the main flanges is another 4 inches and then the chamber is pinched to a neck 10 inches high. This is welded to a section 6 inches in diameter and 3 inches high which, in turn, is mated to an Ultex 100 liters/sec Vacion pump. At the top of the bell jar is a Varian nude ion gauge and a 1-1/2 inch viewing port. Attached to the bell jar are two 6-inch diameter blanked-off access ports, 90° apart, and two 4-inch viewing ports, also 90° apart. All ports have metal-to-metal seals. Below, around the circumference of the bell jar, are four high-power leads, two water leads, and two multiple-pinned feedthroughs. In the 10-inch diameter section is located, horizontally, a Varian titanium sublimation pump rated at 3000 liters/sec, and a roughing port closed off with a high-vacuum metal-to-metal valve 1-inch in diameter and made by Granville-Phillips. On the low-vacuum side of the valve are two Viton-O-ring-sealed ball valves. One leads to the initial roughing system, which in our case was the house vacuum system, and the other to a Varian Sorption pump chilled in liquid nitrogen.

The whole high-vacuum part of the system was baked out at 400°C for about 3 days. Ultimate pressure without the sublimation pump was



MUB 10039

Fig. 5. Schematic of vacuum system.

6.8×10^{-10} torr. With the sublimation pump the pressure was less than 2×10^{-11} torr, the lower limit of the ion gauge. These values are for the vacuum system without the diode.

Also pictured in Fig. 6 is the micro-optical pyrometer used to determine the emitter temperature. It was calibrated against a secondary standard of the National Bureau of Standards. Readings were also taken with and without the window in place to determine a correction for it. The composite calibration curve giving true temperatures from brightness readings is shown in Fig. 7.

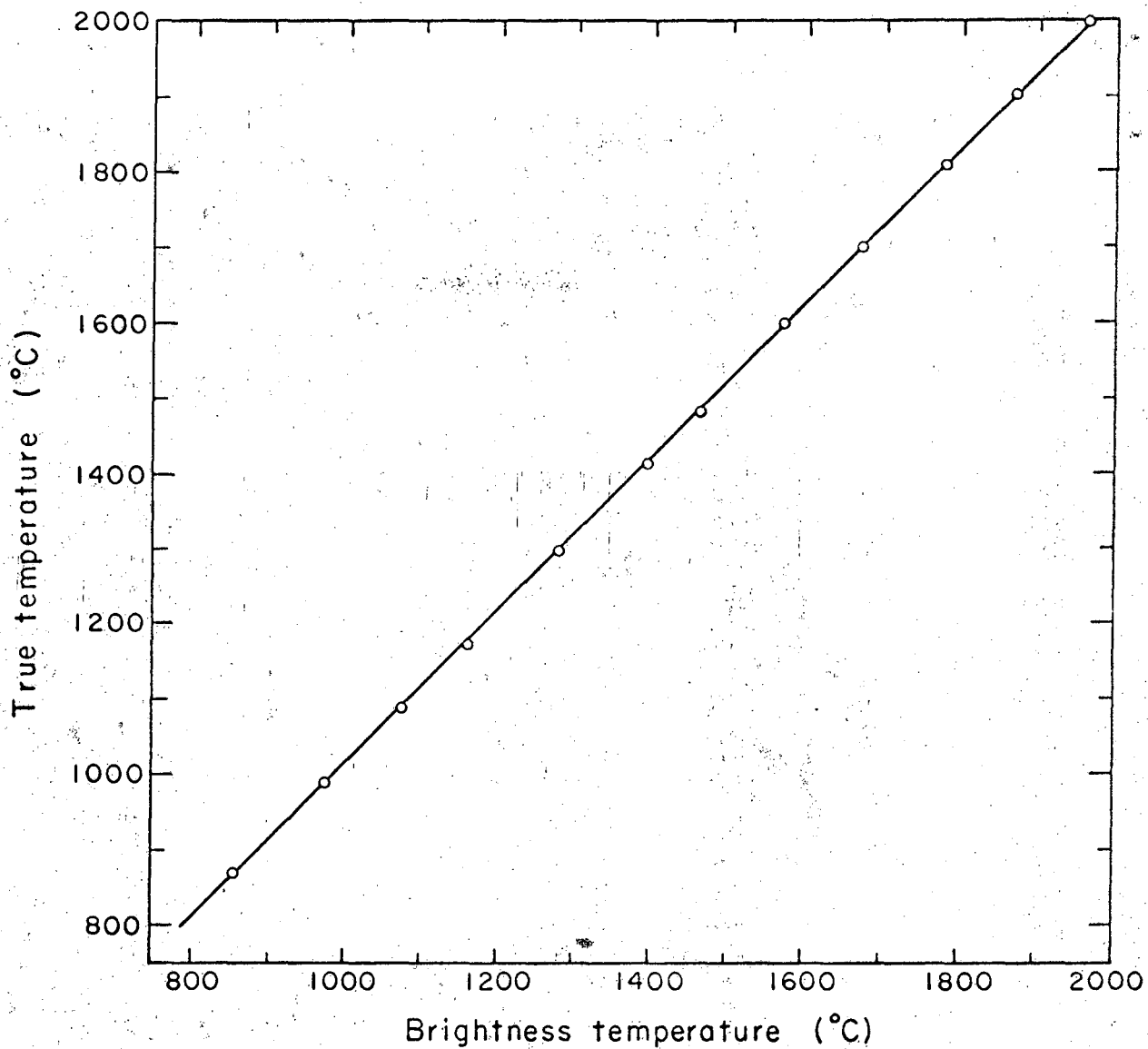
The diode was supported on a pedestal inside the bell jar. A schematic of the diode is shown in Fig. 8. Above the filament is a tantalum cup with the tungsten crystal brazed onto it. Above are the copper crystals brazed onto their respective mountings. The guard ring and collector are electrically insulated from one another and the whole collector assembly is water cooled, not shown, to maintain a constant temperature. Around the base of the tantalum cup is a ceramic pedestal for positioning the three tungsten heat shields. After cold determination of the electrode spacing, the ceramic is raised and the stainless steel blocks positioned, also not shown. The gap is measured to within 0.01 mm with a Gaertner cathetometer.

The single-crystal collector and guard ring were prepared from a (100) oriented copper rod rated as 99.9% pure from Semi Elements, Inc. Wafers approximately 3/16-inch thick were cut off with a Servomet spark cutter. The faces were then lapped flat and parallel, and x-ray pictures were taken to ensure the proper orientation. The wafers were then chemically polished, and finally electropolished. They were then cut into their respective parts and vacuum brazed to their mountings in an auxiliary



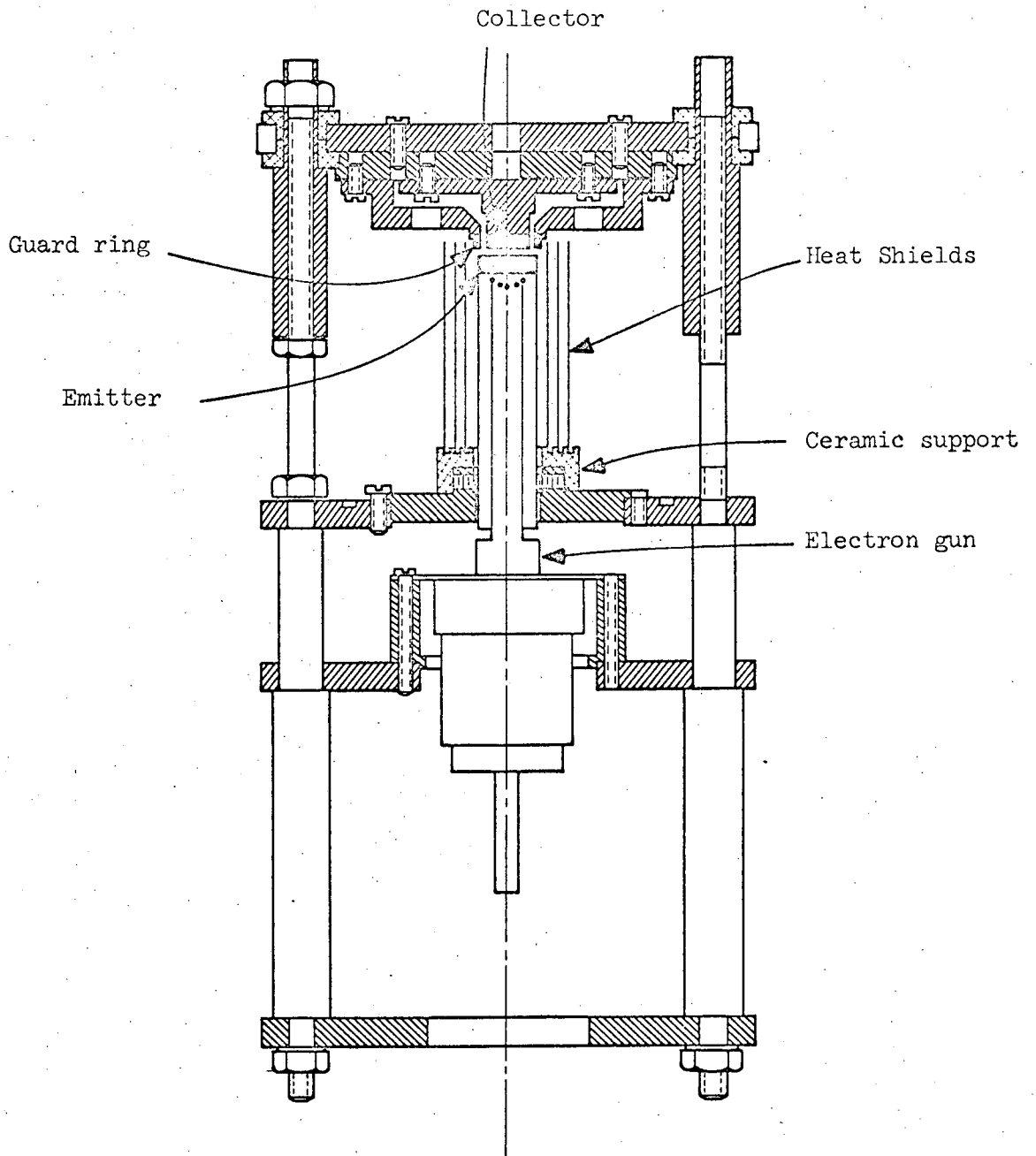
ZN-5575

Fig. 6. Thermionic emission diode and instrumentation stand.



MUB-10641

Fig. 7. Brightness temperature (as measured with pyrometer) versus true emitter temperature, which contains calibration corrections for the pyrometer and a correction for the Pyrex window through which the emitter was observed.



MU-36621

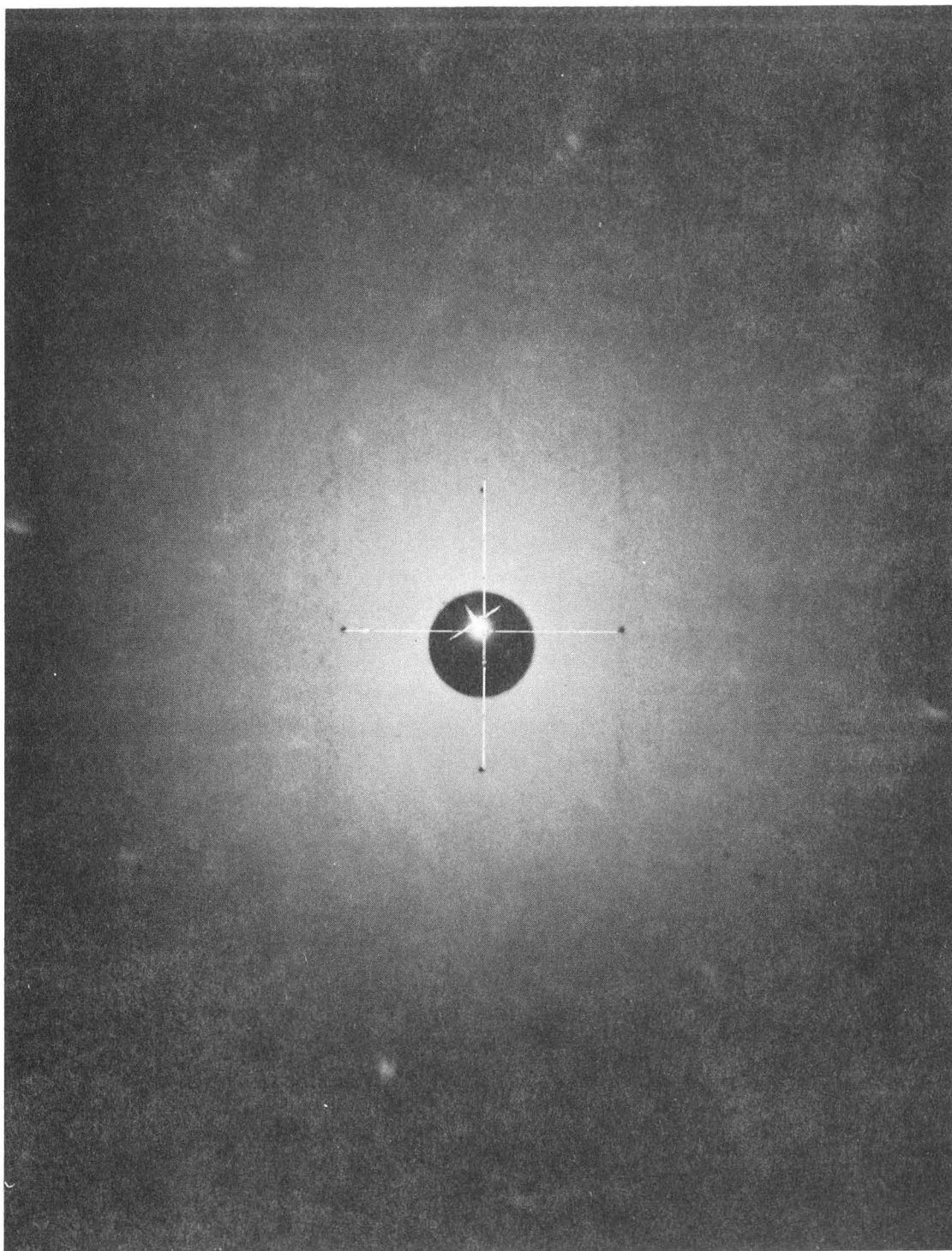
Fig. 8. Schematic of the thermionic diode

vacuum system, using nicusil 3 as the braze alloy. The final x-ray picture of the copper (100) crystal is shown in Fig. 9. For further details see Appendix B.

The (110) and (111) tungsten emitters used in this experiment were prepared by Daniel Koenig. The following is a brief description of their preparation. For more details see Reference 10.

Both the (110) and (111) crystals were cut from roughly cylindrical single-crystal stock $5/8$ to $3/4$ in. in diameter and several inches long, oriented with the (110) direction within 3° of the rod axis. The crystal stock was manufactured by Linde Co., Crystal Products Division.

A 1-in. section of the stock crystal was ground on a lathe to a final diameter of 0.524 in. All subsequent cutting of the crystal, including drilling the blackbody hole, was done under kerosene with the spark cutter to minimize surface deformations. Several wafers of each orientation were cut and then ground optically flat on a precision ceramic lapping wheel with a suspension of Al_2O_3 powder in oil. The faces of each wafer were made parallel to within 0.0001 in. One face of the wafers was electropolished for 20 to 30 minutes, which was sufficient to remove several mils of metal. Great care was taken to maintain the flatness of the crystal face being electropolished. To this end, a polycrystalline tungsten annulus acting as a guard ring was cemented around the wafer. This procedure results in a very well polished, flat surface, although not optically flat. The surface has an "orange-peel" finish characteristic of the electropolishing process. The crystals then were brazed to their tantalum support by inserting a 2- to 4-mil thick molybdenum foil between the two and heating the crystal in vacuum to $2750^\circ C$. The crystals were again generally electropolished to eliminate the slight

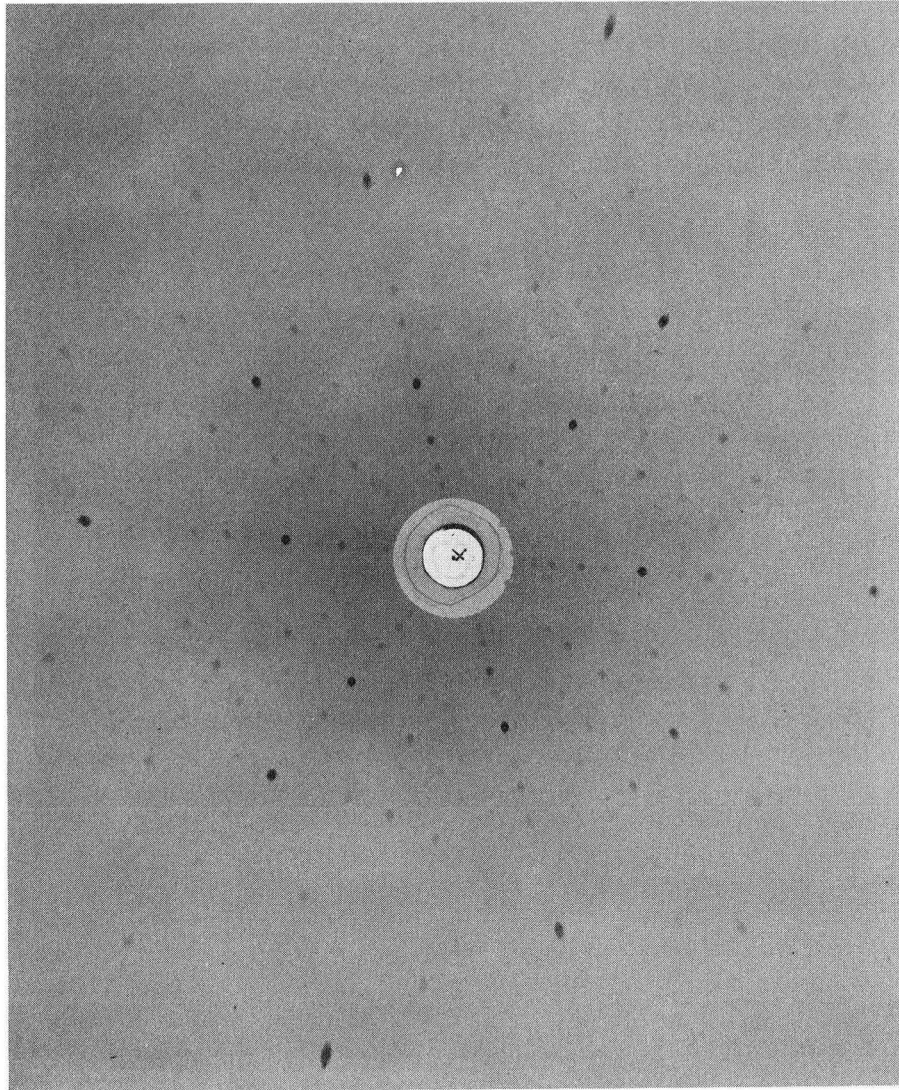


ZN-5576

Fig. 9. Laue pattern of (100) copper single crystal.

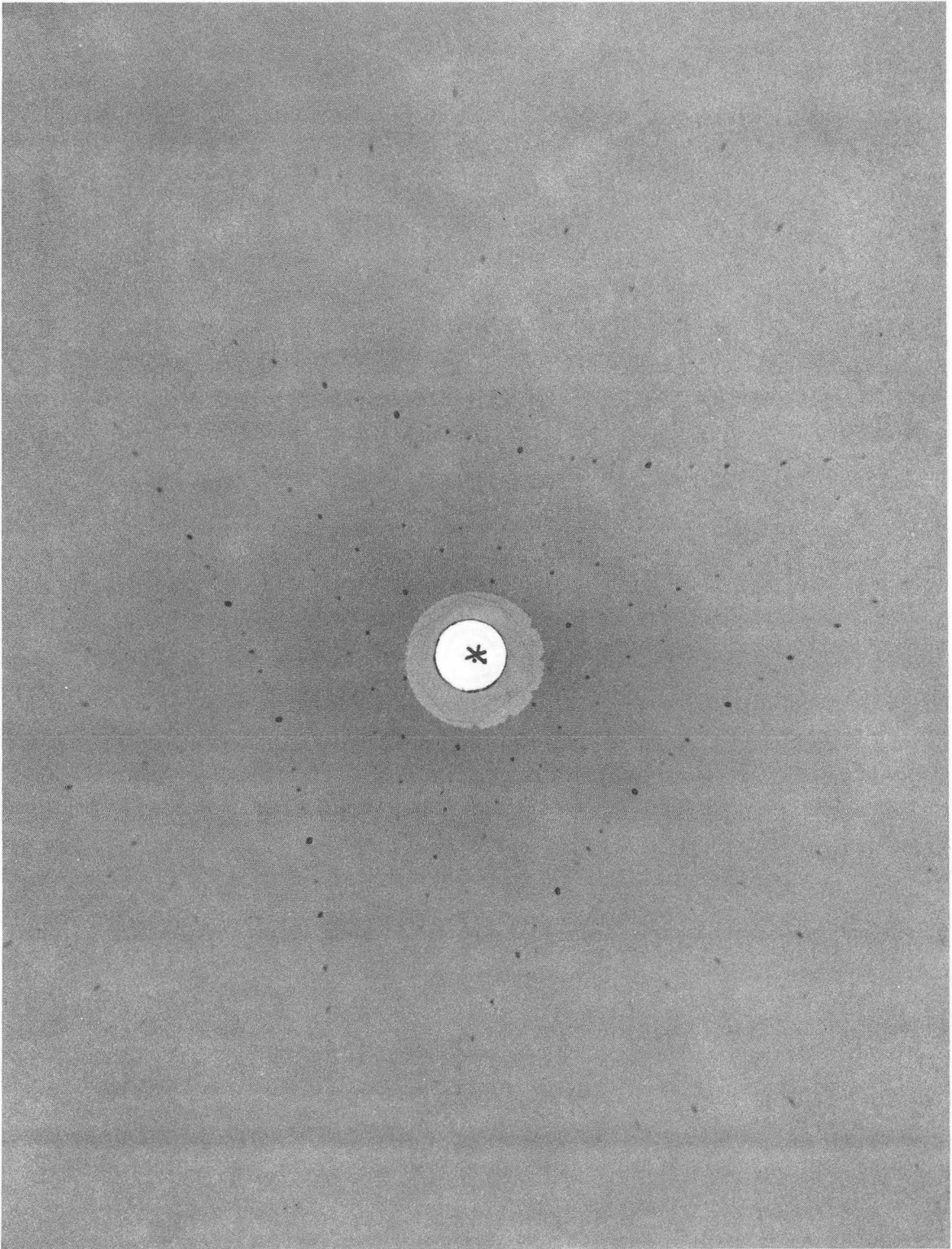
surface deformations which sometimes occurred during brazing.

The orientation of the crystals was measured and adjusted at various stages of the process described above. The orientation of the crystal lattice relative to the surface normal was measured by taking x-ray Laue patterns. Figures 10 and 11 show the Laue patterns of the (110) and (111) emitters, respectively taken normal to their surface just prior to their insertion in the diode. For both, the surface normals lie within less than 1° of the desired lattice orientation.



ZN-5577

Fig. 10. Laue pattern of (110) tungsten single crystal.



ZN-5578

Fig. 11. Laue pattern of (111) tungsten single crystal.

IV. EXPERIMENTAL PROCEDURE AND CIRCUITRY

Prior to the actual data run, the emitter was brought up to full power (approximately 1960°C) and allowed to outgas for one hour. This resulted in a base pressure in the system of about 5×10^{-10} torr. The water coolant was not run at this time to allow the collector and guard ring to heat up to 250°C and 300°C, respectively.

All electronics were left on overnight to stabilize. For the actual run the emitter was brought up to full power, again with no coolant flowing. The coolant was then turned on and varied during the entire run to maintain the collector temperature constant to within 30°C. At full power the pressure rose to approximately 8×10^{-9} torr. Data was taken as the emitter temperature was lowered. At each setting the temperature was allowed to stabilize for 25 minutes. Gap thickness, emitter temperature, system pressure, and thermocouple readings of various parts of the system were taken, i.e., collector and guard ring. Current-voltage readings were taken and at the end of the run the emitter temperature was again taken. The emitter was then lowered to the next temperature and the procedure repeated.

Before and after the entire run a zero-power-leakage current check was made to correct all the data for leakage currents.

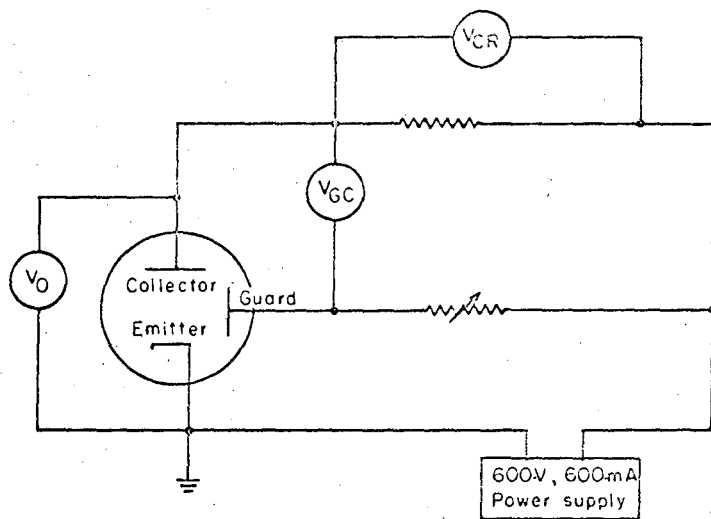
As shown in Fig. 6, the electronics consisted of three power supplies, a digital voltmeter, a precision resistor switching box, and an amplifier unit.

A power supply, NJE model CR-36-20, heated the filament to 10.5 amperes at 7.1 Volts. The filament heated up the emitter by electron bombardment. The NJE was coupled to a Regatron power supply, model No. 209B, which was used as an accelerating voltage between the filament and the grounded emitter. At full power the power supply put out 600 V and approximately

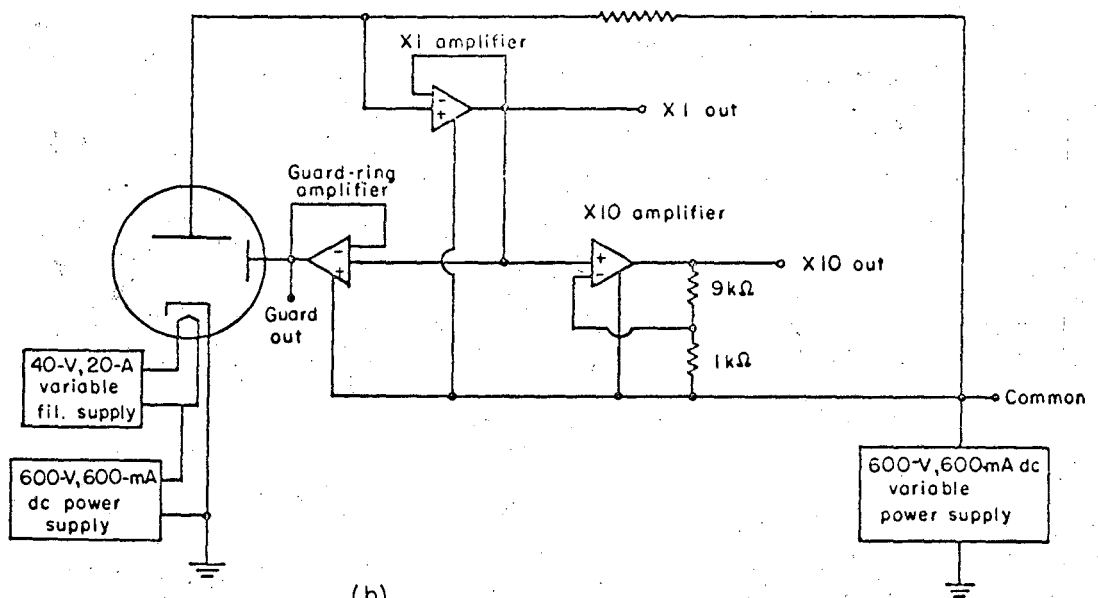
290 mA (depending on the gap between the filament and the tantalum support cup for the emitter). The third power supply, a programable Regatron, model 235AMK, supplied a potential between the emitter and collector.

A digital voltmeter (Dana model 5603), was used for reading the voltages across the diode; it is accurate to 0.01%. The current was calculated by reading the voltage across precision resistors accurate to 0.05%.

The collector and guard ring were maintained at the same potential by a separate amplifier which sensed the voltage difference between the guard ring and collector and kept this difference to less than 500 μ V. A schematic of the circuit is shown in Fig. 12.



(a)



(b)

MUB-10984

Fig. 12 Schematic of (a) meter positions; (b) the electronic circuit

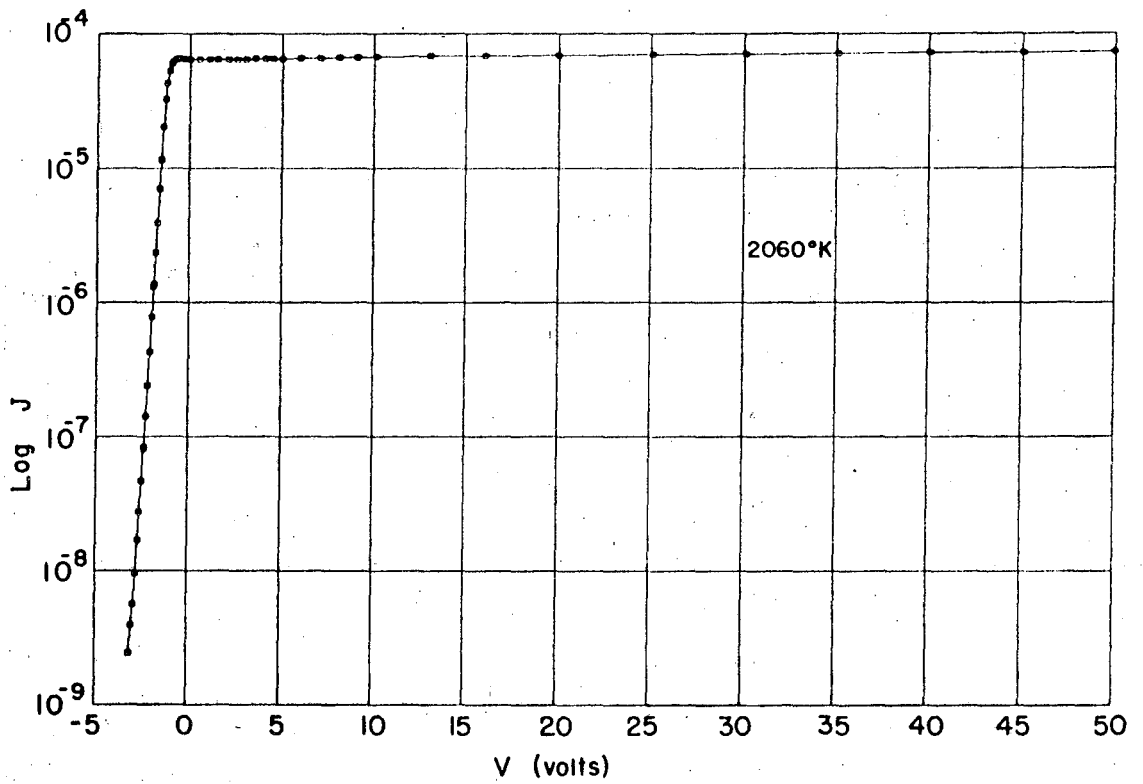
V. PRESENTATION AND DISCUSSION OF RESULTS

A set of vacuum current-voltage curves was obtained for the (110) and the (111) crystallographic orientations of tungsten. Each set of data consisted of I-V curves taken as the emitter temperature was lowered from its maximum value. For illustration we include here the log I-V curve for the (110) crystal at an emitter temperature of 2060°K. Figure 13 shows the data for the entire voltage range, -5 to 50 Volts. Figure 14 is an expanded plot of the -5 to 1 Volt range.

Several features of these curves are indicative of all the data obtained. They are the deviations of the data points from the lines drawn in the retarded potential region, the slope of this line, the position of the saturation line relative to the data points, the sharpness of the transition (the knee) relative to the data points, and the shift of the contact potential with temperature.

For large negative voltages the currents appear to be greater than they really are because the noise level of the instruments was 10^{-9} A. The instrument noise is probably due to leakage current between the guard ring and the collector through the operational amplifier. In calculating the slope of the retarded region in particular, and all calculations in general, we used the THERM code, discussed in Appendix C. In the retarded region, we did a least-squares analysis over the straight portion of the curves above the region where the noise level could have any effect. For the high-temperature runs where the currents were orders of magnitude greater than the noise level, the least-squares analysis encompassed nearly all of the retarded region.

From the slope of the lines in the retarded region, the theoretical electron temperatures were calculated. In all cases they were greater



MU-10981

Fig. 13 (110) tungsten I-V curve for 2060°K.

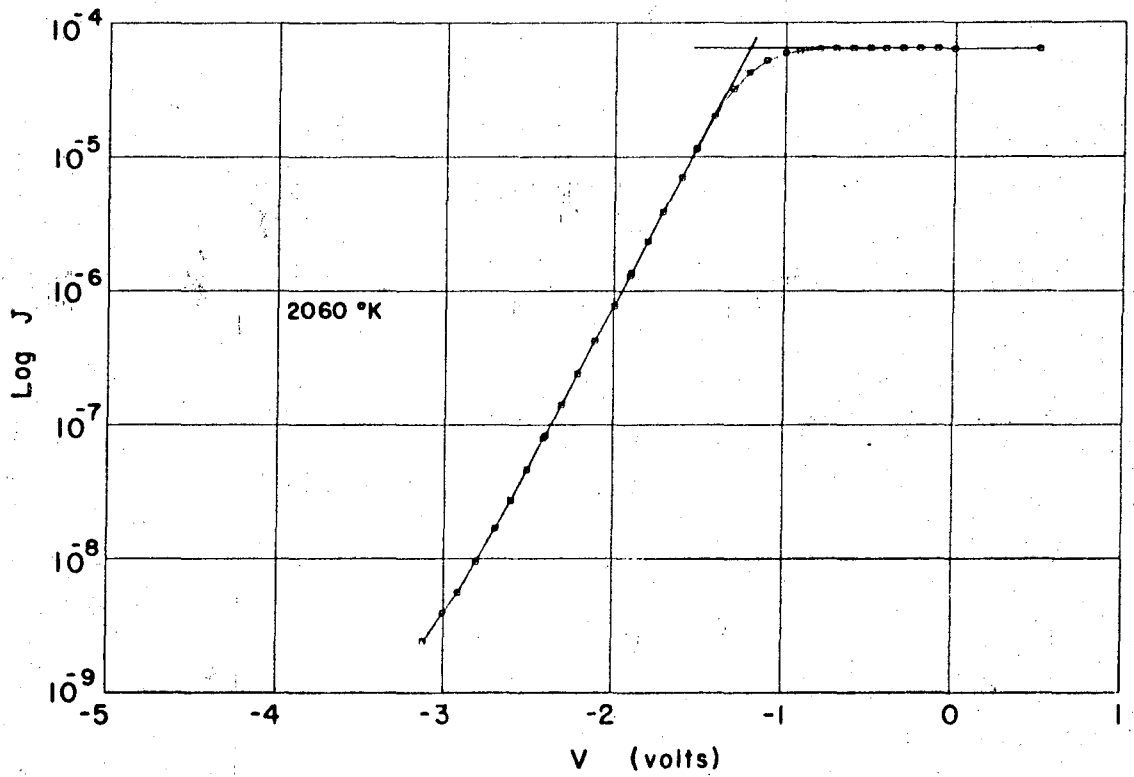


Fig. 14 Expanded (110) tungsten I-V curve for 2060 °K.

MUM-10982

by 2 to 95°K for the (110) and 65 to 115°K for the (111) than the experimentally determined temperatures. These slopes were calculated within 0.5% for the (110) and 0.4% for the (111). We believe that this temperature difference is greater than any reasonable systematic error in the absolute values of the temperature measurements or in the measurements of currents and voltages. Two possible explanations can account for these differences. One is the nonuniformity of both the emitter and collector work functions. The second is the cooling effect accompanying thermionic emission from a uniform surface.¹⁴ Hence, we will be able to rely only on the saturation currents to calculate the emitter work function and Richardson constant A. The Shelton plot is valid only when the two temperatures are equal and for these runs is not applicable.

Figure 15¹ is a Schottky plot for the above I-V curve. It more clearly shows the deviation of the data from a straight line close to the knee. Aside from the drop-off of the data points at very low fields due to space charge and field inhomogeneities, the small variation at low fields resembles Bragg reflection, is sensitive to exact surface, and remains unexplained.¹⁸ In drawing the saturation line on the Schottky plot, we made a least-squares analysis, using data far enough away from the knee to represent purely saturation effects.

Space charge is dependent on both the spacing of the interelectrode gap and the magnitude of the emission current. For very low temperature emission, the currents are very small but the gap size is greater. For very high temperature emission, the currents are very large but the gap size is smaller due to thermal expansion of the tantalum cup. For the two runs taken, the gap varied by 5 mils, being 4 mils at its smallest point (the highest temperatures). The magnitude of the gaps is enough

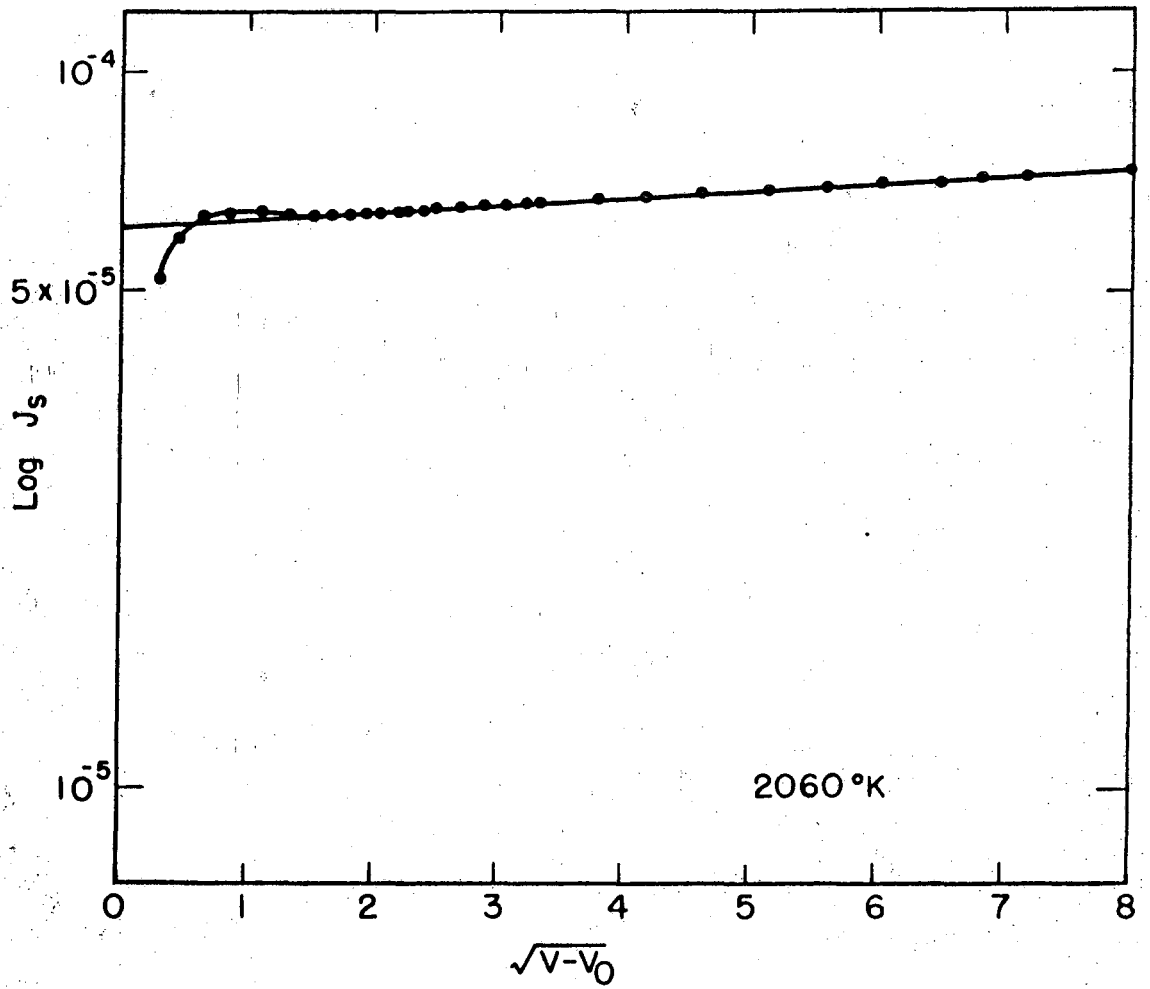
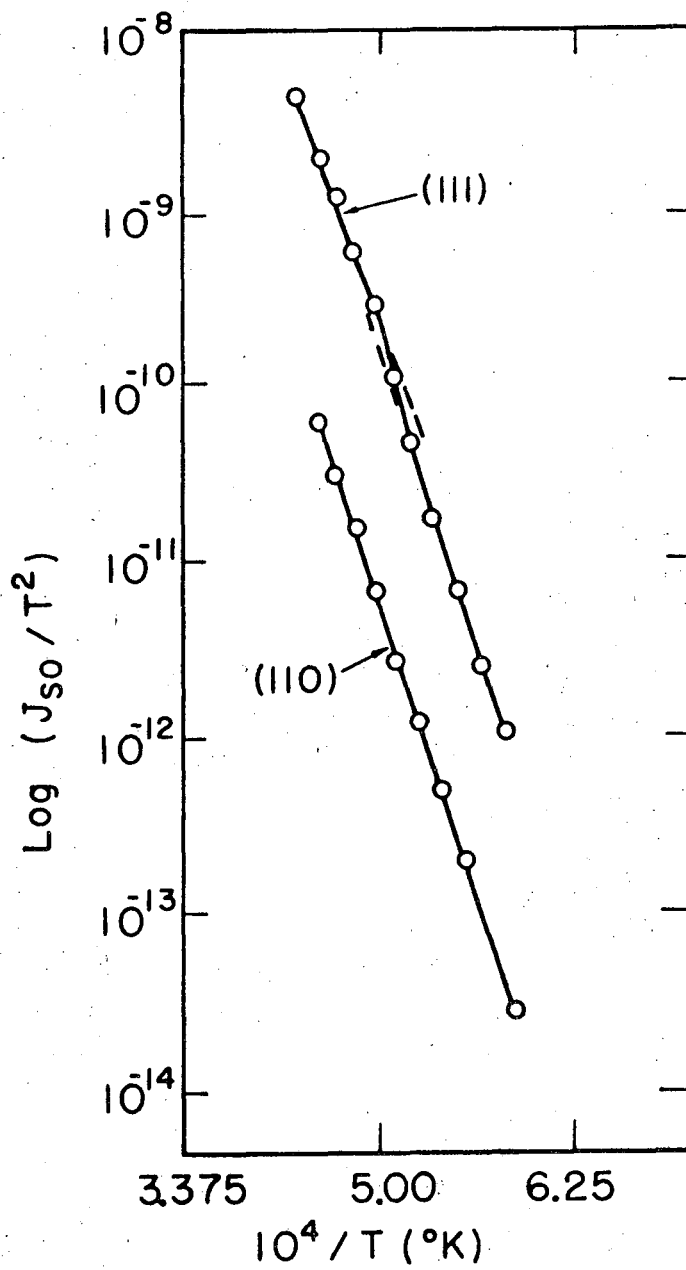


Fig. 15 (110) tungsten Schottky plot for 2060°K.

MUB 10983



MUB-10985

Fig. 16 Richardson plots for (110) and (111) tungsten.

to account for some rounding of the knees throughout the run. And the other two competing effects explain the greater degree of rounding at both extremes of emission.

For the (110) crystal the shift of the knee with temperature was not observed, within experimental accuracy, as seen from Table I; however, for the (111) crystal the shift of the knee was more pronounced, as seen in Table II. This is explainable by a temperature dependence of the (111) work function of $-2 \times 10^{-4} \pm 1 \times 10^{-4}$ V/°K. This value was calculated from $V = -V_o = -\phi_c + \phi_{eo} + \alpha T_e$, by plotting V_o versus T_e and determining the slope. Here α is on the order of the values quoted in the literature. Fine et al.¹⁹ quote a value of -1.4×10^{-4} V/°K for the (110) orientation and comment that it is on the order of $\pm k$, 0.86×10^{-4} V/°K, as predicted by Herring and Nichols.¹⁴ Though temperature dependences vary with crystallographic orientation, magnitudes are roughly the same.

The Richardson plots shown in Fig. 16 were constructed with the saturated current densities found from the Schottky plot and the experimentally determined temperatures. The THERM code calculated A_R and ϕ_{eo} and their respective standard deviations. For the (110) data all points were used in the calculation, but for the (111) data the regions above and below the transition temperature were analyzed independently. The data are tabulated in Table III. Note that the standard deviations were calculated on the basis of $1/(N-2)$, where N is the number of points and 2 was the number of free parameters fitted. For small populations such as ours, this ratio yields fairly conservative estimates of the standard deviation.

The (110) data were quite good and ϕ_{eo} was calculated within 0.2% to be 5.219 ± 0.01 V; A_R was calculated within 8% to be 86 ± 7 amperes/cm²-°K².

Table I. Tungsten (110) work function calculated from Richardson equation with $A = 120 \text{ A/cm}^2\text{-}^\circ\text{K}^2$ and copper (100) work function calculated from the contact potential and ϕ_{eff} .

Temperature ($^\circ\text{K}$)	ϕ_{eff} (V)	$-V_o$ (V)	$\phi_{c;\text{eff}}$ (V)
2163	5.28	1.21	4.07
2113	5.28	1.21	4.07
2060	5.28	1.20	4.08
2006	5.28	1.21	4.07
1953	5.28	1.21	4.07
1900	5.27	1.21	4.06
1850	5.28	1.21	4.07
1798	5.28	1.21	4.07
1697	5.27	1.20	4.07

Table II. Tugsten (111) work function calculated from Richardson equation with $A = 120 \text{ A/cm}^2 \text{-}^\circ\text{K}^2$ and copper (100) work function calculated from the contact potential and ϕ_{eff} .

Temperature ($^\circ\text{K}$)	ϕ_{eff} (V)	$-V_o$ (V)	$\phi_{c,\text{eff}}$ (V)
2237	4.64	0.20	4.44
2155	4.62	0.20	4.42
2114	4.63	0.21	4.42
2061	4.64	0.21	4.43
2013	4.65	0.23	4.42
1963	4.69	0.27	4.42
1918	4.73	0.30	4.43
1868	4.76	0.32	4.44
1816	4.77	0.35	4.42
1767	4.79	0.34	4.45
1717	4.79	0.35	4.44

Table III. Thermionic parameters calculated from THERM code by means of Richardson plot.

Crystal Orientation	ϕ_{eo} (V)	A_R (amperes/cm ² - °K ²)
(110)	5.219 ± 0.01	86 ± 7
(111) above transition	4.74 ± 0.15	214 ⁺²⁴⁴ - 114
(111) below transition	5.28 ± 0.11	3262 ± 3262

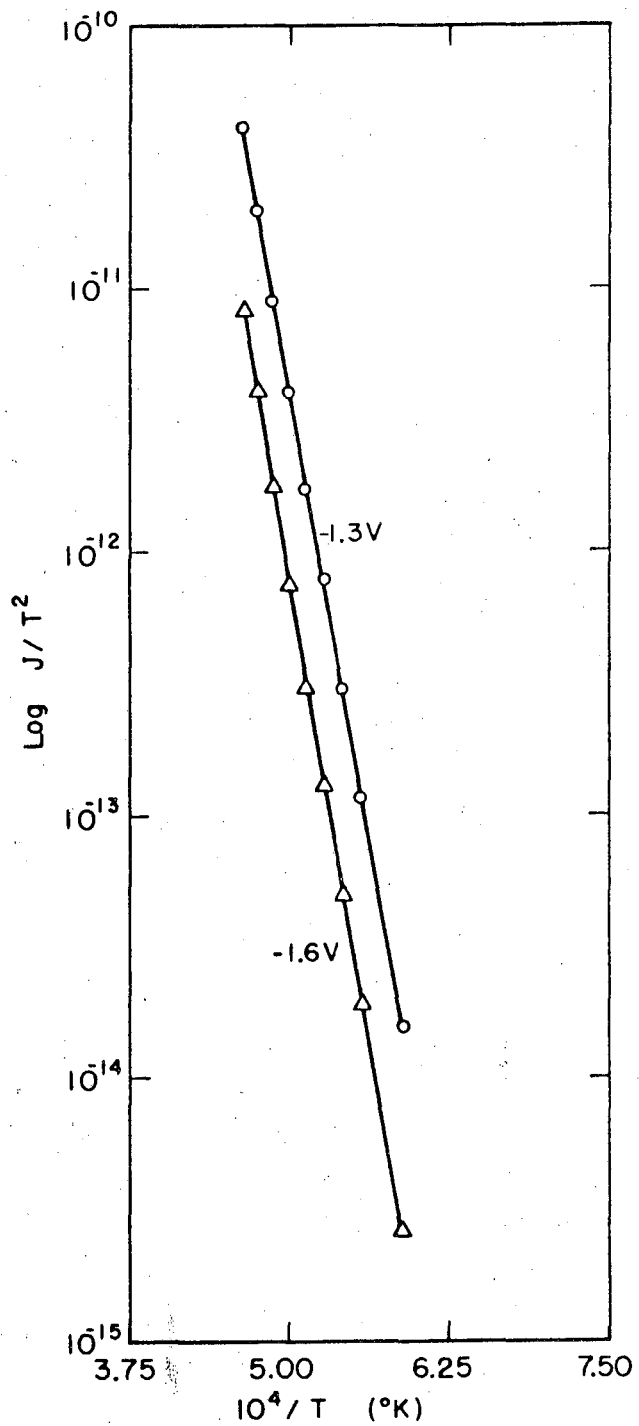
As pointed out by Koenig,¹⁰ the error quoted for ϕ_{eo} is reasonable because the evaluation of ϕ_{eo} is practically independent of a systematic error in the measurement of T_e arising from uncertainties in the effective emissivity of the hohlraum and the adsorptivity of the windows. It is also independent of a systematic error in the current measurement that is directly proportional to the value of the current. On the other hand, the evaluation of A_R is very sensitive to these two types of errors. However, the voltmeter and the precision resistors were well calibrated and any error in A_R resulting from a systematic error in the current measurement was small. For A_R a third possible error is the determination of the surface area of the collector. Since there is also a 10-mil gap between the collector and the guard ring, half the gap was added to the collector area.

For the (111) run a transition occurred at about 2000°K (Fig. 16). This phenomenon has been reported by Koenig,¹⁰ Sytaya,⁹ and Becker and Brandes²⁰ and is attributed to adsorption on the tungsten emitter. The

most likely cause is oxygen. Sytaya concluded that the threshold of oxygen adsorption on the (100) surface is 2100°K; that for the (110) surface about 2000°K. However, according to Becker and Brandes, oxygen adsorption starts around 1600°K for the (100) surface, and roughly 1800°K for both the (110) and the (111) surfaces. Although the magnitudes of the results from the two authors differs, the order of which surface will adsorb first is reversed. The important thing is that oxygen does adsorb onto tungsten and this adsorption does increase the work function. In view of this, and following the example of Koenig, the (111) data were analyzed in two parts, with the high-temperature part above the transition yielding the pertinent (111) tungsten data. Table I shows the data for both regions; for the (111) crystal ϕ_{eo} was calculated within 3.1% to be 4.74 ± 0.15 V and A_R within 11.4% to be $214 \begin{matrix} +244 \\ -114 \end{matrix}$ amperes/cm²-°K² for above the transition. The sensitive dependence of A_R on various factors is reflected in the uncertainty with which it was calculated.

Finally, a Shelton plot was made (Fig. 17) with the calculations from the THERM code. These values are given in Table IV. As can be seen, not only did the work function of the collector vary with greater negative voltages, but the A^* values also changed quite radically, showing its sensitivity. Data for the (111) crystal are for above the transition temperature. The temperature dependence on ϕ_e could not be calculated from A^* and A_R because the proper A^* to use was not known.

In Tables I and II the effective emitter work function, ϕ_{eff} , for both crystals are based on the experimentally determined currents and an A of 120 amperes/cm²-°K². Also listed are the contact potentials and the effective collector work functions calculated from the given data. For these calculations the full range of values was given for the (111) crystal.



MUB-10986

Fig. 17 Shelton plots for (110) tungsten.

Table IV. Thermionic parameters calculated from THERM code by means of Shelton plot.

$-V$ (V)	(111) ϕ_c (Volts)	(111) A^* (amperes/cm ² -°K ²)	(110) ϕ_c (Volts)	(110) A^* (amperes/cm ² -°K)
0.2	4.25	47	-	-
0.3	4.23	43	-	-
0.4	4.20	39	-	-
0.5	4.18	35	-	-
0.6	4.16	32	-	-
0.7	4.14	29	-	-
0.8	4.12	26	-	-
1.0	4.08	22	-	-
1.3	-	-	4.01	90
1.4	3.99	15	-	-
1.6	-	-	3.89	46
2.0	3.86	8	-	-

The rise in ϕ_{eff} for the (111) crystal is indicative of a contaminated surface and was expected in view of the above discussions. For the (110) crystal, ϕ_{eff} remains essentially constant over the entire temperature range. As can be seen, the $\phi_{c,\text{eff}}$ remained essentially constant for each run. This is due to the water cooling of the collector assembly. A possible explanation why the $\phi_{c,\text{eff}}$ of the (111) run is different than that for the (110) is that the collector was not touched between runs and thus started out with a different surface condition. The bare work function for (100) copper is 5.61 V, as found by Underwood in 1935.²¹ Our values are 4.07 and 4.43 V.

The difference in our values for the two runs is easily explained by surface contamination. It is interesting, though, that the only reference on the work function of (100) copper found in the literature is Ref. 21, and the measurement is photoelectric, not thermionic.

VI. CONCLUSIONS

1. The (110) tungsten bare work function was found to be

$$5.219 \pm 0.01V,$$

with a corresponding Richardson constant of

$$86 \pm 7 \text{ amperes/cm}^2 \text{-}^\circ\text{K}^2.$$

2. The (111) tungsten bare work function was found to be

$$4.74 \pm 0.15 V,$$

with a corresponding Richardson constant of

$$214 \pm 244 \text{ amperes/cm}^2 \text{-}^\circ\text{K}^2$$

and a temperature dependence of

$$-2 \times 10^{-4} \pm 1 \times 10^{-4} \text{ V/}^\circ\text{K}.$$

3. A bend in the (111) Richardson plot could be explained by oxygen adsorption at a threshold temperature of about 2000°K .
4. No temperature dependence or gaseous adsorption effects were observed on the (110) surface of tungsten.
5. The work function of (100) copper was found to be 4.07 and 4.43 V, but neither value is felt to be the true bare work function of (100) copper because of contamination of the collector surface.

ACKNOWLEDGEMENTS

I wish to express my appreciation to Professor Thomas H. Pigford for his advice and encouragement during the course of these experiments. A special debt of gratitude is owed to Dr. Daniel R. Koenig, a fellow graduate student, who not only suggested this thesis but rendered invaluable assistance and helped see it to fruition. I also personally thank Ronald Wichner, another fellow graduate student, who helped make possible the early completion of this thesis by assisting in the design and assembly of the experimental apparatus. The expert vacuum system was engineered by Leonel S. Stollar and many parts of the diode and instrumentation stand were built in the Nuclear Engineering Department Mechanical and Electrical Shops under his supervision.

I wish to thank the National Science Foundation for their financial assistance during the course of this investigation.

This research was sponsored in part by the United States Atomic Energy Commission and in part by the National Aeronautics and Space Administration.

APPENDICES

A. Nomenclature

<u>Symbol</u>	<u>Usage</u>
A	theoretical Richardson constant = $120 \text{ amperes/cm}^2 \text{-}^\circ\text{K}$
A_R	Richardson constant calculated from Richardson plot
A^*	true temperature-dependent A calculated from Shelton plot
e	charge on electron
F	Fermi level
F_c, F_e	Fermi level in collector and emitter, respectively
F_o	applied field at emitter surface
J, J_s, J_{so}	current density, saturated current density, saturated current density at zero applied field
k	Boltzmann constant
\bar{r}	average reflection coefficient for electrons at emitter
T, T_e	temperature and emitter temperature in $^\circ\text{K}$
V, V_a	externally applied, interelectrode voltage
V_o	contact potential voltage = $\phi_c - \phi_e$
W	height of potential barrier at surface of a metal
α	postulated temperature dependence of $\phi_e = d\phi_e/dT_e$
δ	space charge barrier
$\phi_c, \phi_e, \phi_{eo}$	work function of collector, emitter, and emitter at 0°K , respectively
$\phi_{eff}, \phi_{c,eff}$	effective work function of emitter and collector calculated on the basis of $A = 120 \text{ amperes/cm}^2 \text{-}^\circ\text{K}^2$

B. Preparation of Single-Crystal Copper Collector and Guard Ring

The (100) oriented single crystal of copper, obtained from Semi-Elements Inc., is rated as 99.9% pure. It comes in a 1-inch diameter rod 4 inches long, oriented with the (100) direction within 2° of the rod axis. A wafer $13/64$ -inch thick was cut off with a spark cutter (Metals Research Ltd., Servomet) to minimize surface deformations. The wafer was then ground optically flat on a precision ceramic wheel with a suspension of Al_2O_3 powder in oil. The wafer was washed in a Stoddard solvent sonic bath to dislodge any suspension from the surface. An x-ray Laue pattern was taken and the orientation of the crystal lattice relative to the surface normal of the ground face determined to lie within 1° of the desired orientation. The rough side of the wafer was then ground parallel to the reverse face to within 0.0001 inch and the wafer reduced to a thickness of 0.170 inch. The wafer was again washed in the Stoddard solvent sonic bath and then chemically polished for one minute in a solution of 1 part nitric acid, 1 part acetic acid, and 1 part orthophosphoric acid, leaving a flat reflecting finish.

One face of the wafer was electropolished for 30 minutes, which was sufficient to remove several mils of metal. Copper was used for the negative electrode. The electropolishing solution was at room temperature and consisted of 50 mls distilled water, 100 mls orthophosphoric acid, and a few drops of molasses. Molasses was found to aid in forming the surface film on the wafer face, thus retarding the current and producing a more uniform polish. Best results occurred for an applied voltage of 1.8 Volts at a current of about 0.19 amperes/cm². This procedure resulted in a very well polished, flat surface, although not optically flat. The surface had an orange-peel type of finish characteristic of the electropolishing process.

The 0.364-inch diameter collector crystal was then spark-cut out of the wafer with a circular brass cutting tool with a 30-mil wall. For the guard ring, the brass cutting tool consisted of two concentric 30-mil walls cutting out the guard ring to a 0.524-inch outside diameter and a 0.384-inch inside diameter. This leaves a 10-mil gap between the collector and the guard ring.

The crystals were then brazed to their respective OFHC copper mountings in an auxiliary vacuum system. The braze alloy was nicusil 3 (71.15% Ag, 28.10% Cu, 0.75% Ni), which has a melting point of 795°C. The melting point of the collector was visually noted. However, the temperature of the guard ring was monitored with a thermocouple to determine whether or not the nicusil had melted. The latter technique was necessitated by the design of the guard ring mounting as shown in Fig. 8.

Finally, the crystals were re-electropolished for 10 minutes each to compensate for the dulling of the polish from the spark cutting and the brazing.

A final Laue pattern was taken of the collector, Fig. 9, just before it was mounted in the diode to ensure that the data would correspond to the desired orientation.

During the bakeout of the entire vacuum system, the collector temperature reached a high of about 290°C. During the actual run the emitter was brought up to full power and the collector temperature reached a high of about 250°C, with no coolant flowing through the collector assembly. Comparable readings for the guard ring were 325°C and 300°C. That these temperatures, however, are not nearly high enough to clean off the collector is shown by the collector work function calculated for the various emitters. To properly clean off the collector would have required our reaching temperatures comparable to the melting point of copper.

C. THERM Code and Random Errors

A computer code, written by Edna Williams (LRL), took thermionic emission data as input and printed out all essential thermionic constants with their respective standard deviations. The code was originally written for the IBM 7094, but has been converted for the CDC 6600. In its present form the code is known by THERM 75. Provision is also made for having the data graphically shown by Cal-comp plotter.

Input:

- Card 1: Number of Shelton plots to be made, up to 10.
- Card 2: Retarded region potentials used for Shelton plots.
- Card 3: Temperature of emitter, noise resistance, maximum and minimum voltage values used for plotting I-V curves, area of collector, and number of vertical grid lines on I-V plot.
- Card 4: Minimum and maximum retarded region potentials for I-V plot, and minimum and maximum saturated region potentials for I-V and Schottky plots.
- Card 5: Voltage across known resistor, voltage, and resistance.

Card 4 specified the range of values needed to compute a least-squares analysis for the retarded region, the saturated region, and the Schottky plots. Card 3 sets down the vertical grid for the I-V plots. The program sets the horizontal grid by decades of 10 (ln plot) by reading the input and starting the plot one decade below the lowest value and one decade above the highest value.

The program then performs a least-squares analysis over the retarded region and computes the electron temperature from the slope along with its standard deviation. The program also does a least-squares fit for the saturated region and solves the two calculated lines for the intercept, V_0 , and an

accompanying deviation. The Schottky plot is then drawn with the respective calculated V_o , and a least-squares fit is made to it. The intercept is then given, J_{so} , and an accompanying deviation. The respective J_{so} 's are then used to calculate a Richardson plot. A least-squares fit is also made and the slope and intercept given with their deviations. Finally the program uses the computed retarded region curves to plot a Shelton plot. A least-squares analysis here also gives the slope, ϕ_c , and the intercept, A^* , and their accompanying deviations.

All standard deviations are done on the basis of $1/(N-M)$ where N is the number of points and M is the number of parameters fitted. In our case M was always equal to 2. Thus all random errors in the data, and thus in the calculations, were accounted for in every significant parameter computed.

REFERENCES

1. M. H. Nichols, The Thermionic Constants as a Function of Crystallographic Direction, Phys. Rev., 57, 297 (1940).
2. J. A. Becker, The Use of the Field Emission Microscope in Adsorption Studies of W on W and Ba on W, Bell Sys. Tech. J., 30, 907 (1951).
3. George F. Smith, Thermionic and Surface Properties of Tungsten Crystals, Phys. Rev., 94, 295 (1954).
4. M. K. Wilkinson, Crystallographic Variations of Field Emission from Tungsten, J. Appl. Phys., 24 (9), 1203 (1953).
5. Erwin W. Muller, Work Function of Tungsten Single Crystal Planes Measured by the Field Emission Microscope, J. Appl. Phys., 26 (6), 732 (1955).
6. Fred L. Reynolds, Surface Ionization on Tungsten Single-Crystal Filaments, UCRL-10618 (1963).
7. James W. Little, T. E. Madey, and R. Klein, Work Function Measurements on Field Emitters with Prescribed Orientation, J. Appl. Phys., 36 (1), 1491 (1965).
8. A. A. Brown, L. J. Neelands, and H. E. Farnsworth, Thermionic Work Function of the (100) Face of a Tungsten Single Crystal, J. Appl. Phys., 21 (1), 1 (1950).
9. E. P. Sytaya, M. I. Smorodina, and N. I. Imangulova, Electron and Ion Emission from the (100) and (110) Faces of a Large Tungsten Monocrystal, Soviet Physics - Solid State, 4 (4), 750 (1962).
10. Daniel Rene Koenig, Surface Ionization of Cesium and Thermionic Emission from Planar Single Crystals of Tungsten, (Ph.D. Thesis), UCRL-11857 (1966).

11. E. Blue and J. H. Ingold, Characteristics of a Thermionic Converter with a High Temperature Collector, General Electric Vallecitos-2011 (1963).
12. Wayne B. Nottingham, Thermionic Emission, in Handbuch der Physik, S. Flugge, Editor (Springer-Verlag, Berlin, 1956), vol. 21, p. 1.
13. N. S. Rasor, Emission Physics of the Thermionic Energy Converter, Proceedings of the IEEE, 733 (1963).
14. Conyers Herring, and M. H. Nichols, Thermionic Emission, Rev. Mod. Phys., 21 (2), 185 (1949).
15. J. A. Becker, Thermionic Electron Emission and Adsorption, Rev. Mod. Phys., 7 (2), 95 (1935).
16. Bernhard A. Rose, Measurements on Contact Potential Difference Between Different Faces of Copper Single Crystals, Phys. Rev., 44, 585 (1933).
17. Albert Van Der Ziel, Solid State Physical Electronics. (Prentice-Hall Inc., Englewood Cliffs, N. J., 1957).
18. Haywood Shelton, Thermionic Emission from a Planar Tantalum Crystal, Phys. Rev., 107 (6), 1955 (1957).
19. Joseph Fine, T. E. Madey, and M. D. Scheer, The Determination of Work Function from the Ratio of Positive to Negative Surface Ionization of an Alkali Halide, Surface Science, 3, 227 (1965).
20. J. A. Becker and R. G. Brandes, On the Adsorption on Tungsten as Revealed in the Field Emission Electron Microscope, J. Chem. Phys., 23 (7), 1323 (1955).
21. Newton Underwood, The Photoelectric Properties of the (100) and (111) Faces of a Single Copper Crystal, Phys. Rev., 47, 502 (1935).

FIGURE CAPTIONS

- Fig. 1 Motive diagram: (a) retarded region, $V_a = V + V_0$; (b) critical point, $V = -V_0$; (c) saturated region, $V_a = V - V_0$.
- Fig. 2 Current-voltage characteristics. (above).
- Fig. 3 Richardson plot. (middle).
- Fig. 4 Schottky plot. (below).
- Fig. 5 Schematic of vacuum system.
- Fig. 6 Thermionic emission diode and instrumentation stand.
- Fig. 7 Brightness temperature (as measured with pyrometer) versus true emitter temperature, which contains calibration corrections for the pyrometer and a correction for the Pyrex window through which the emitter was observed.
- Fig. 8 Schematic of the thermionic diode.
- Fig. 9 Laue pattern of (100) copper single crystal.
- Fig. 10 Laue pattern of (110) tungsten single crystal.
- Fig. 11 Laue pattern of (111) tungsten single crystal.
- Fig. 12 Schematic of (a) meter positions and (b) the electronic circuit.
- Fig. 13 (110) tungsten I-V curve for 2060°K.
- Fig. 14 Expanded (110) tungsten I-V curve for 2060°K.
- Fig. 15 (110) tungsten Schottky plot for 2060°K.
- Fig. 16 Richardson plots for (110) and (111) tungsten.
- Fig. 17 Shelton plots for (110) tungsten.

This report was prepared as an account of Government sponsored work. Neither the United States, nor the Commission, nor any person acting on behalf of the Commission:

- A. Makes any warranty or representation, expressed or implied, with respect to the accuracy, completeness, or usefulness of the information contained in this report, or that the use of any information, apparatus, method, or process disclosed in this report may not infringe privately owned rights; or
- B. Assumes any liabilities with respect to the use of, or for damages resulting from the use of any information, apparatus, method, or process disclosed in this report.

As used in the above, "person acting on behalf of the Commission" includes any employee or contractor of the Commission, or employee of such contractor, to the extent that such employee or contractor of the Commission, or employee of such contractor prepares, disseminates, or provides access to, any information pursuant to his employment or contract with the Commission, or his employment with such contractor.

